UJEAS

UNIZIK JOURNAL OF ENGINEERING AND APPLIED SCIENCES

UNIZIK Journal of Engineering and Applied Sciences 6(3), September (2026), 3860-3869
Journal homepage: https://journals.unizik.edu.ng/index.php/ujeas
PRINT ISSN: 2992-4383 || ONLINE ISSN: 2992-4391

Delineation of Shallow Soil Pipes and Subsidence Zones in Awka South, Anambra Basin, Using Vertical Electrical Sounding and Ground Magnetic Methods

Chibuogwu Ikechukwu Udoka[1], Obichukwu Obiemeka Obiajulu[1], Alor Kenechukwu Perpetual[1], Maureen Chioma Umeh[2] and Obiabunmo Obiora Christian[1]*
[1]Department of Physics and Industrial Physics, Nnamdi Azikiwe University, Awka, Anambra State

[2]Department of Applied Geophysics, Nnamdi Azikiwe University, Awka, Anambra State

**Corresponding Author's E-mail:* iu.chibuogwu@unizik.edu.ng

Abstract

This study employed an integrated geophysical approach using Vertical Electrical Sounding (VES) and ground magnetic surveys to investigate soil pipes in two sinkhole sites in Awka South. The study area lies within the Anambra Basin, underlain by the Imo Shale Formation and dispersive Nanka sands, with soils that are lateritic, acidic and highly erodible. Eighteen VES were acquired using Schlumberger array with AB/2 up to 100 m using PASI resistivity meter and inverted with IPI2Win software. Ground magnetic data were acquired on a 2 m x 2 m grid along 9 profiles using proton precession magnetometer, with diurnal correction and gridding using minimum curvature method. Results show topography strongly controls pipings with Site I characterized by closed depressions (38-58 m elevation) and Site II by an elongated SW-NE crest (>150 m). Magnetic data ranged from -196 to +91 nT in Site I and -374 to +164 nT in Site II. Magnetic highs of +29.5 to +164.0 nT indicate intact ferruginous sandstone and ironstone pipe roofs, while magnetic lows of -124.3 to -374.0 nT delineate leached zones, water-saturated pipes and air-filled voids. VES revealed 3-5 layer resistive-conductive-resistive models with HK, HKH, KHK, AK, AKQ curves. Σρ at <5 m proved diagnostic: very low values of 16.36-66.8 Ωm (VES 7,8,9,13) indicate active pipes, while very high values of 78,549-97,221 Ωm (VES 1,5) indicate non pipes. Piping is shallow at 0.5-3.5 m depth, with roof thickness as low as 0.649 m. Integration confirms pipes form an interconnected SW-NE network controlled by structure and perched aquifer drainage at the Imo Shale/Nanka interface, rendering patching ineffective. The study provides a baseline for engineering remediation.

Keywords: Reconfigurable intelligent surface, covert communication, smart grid, advanced metering infrastructure, smart meters.

1. Introduction

Soil piping is a form of subsurface erosion where dispersive soils are progressively washed away by seepage forces, creating continuous subsurface tunnels or pipes (Chibuogwu and Ugwu, 2023a). Over time, the roofs of these tunnels collapse, leading to sudden surface subsidence, formation of sinkholes and development of large underground cavities. Unlike gully erosion which is visible from onset, soil piping is a concealed process that often gives little or no surface warning before catastrophic failure. This phenomenon has been extensively reported in communities such as Agulu, Nanka, Oko, Awka, Ekwulobia and Isuofia, all located within the Anambra Basin (Nich and Okeke-Ogbu, 2017).

The implications of this development are far-reaching. Soil piping and its resultant subsidence have significantly reduced the agricultural productivity of the state. Farmlands that were once fertile and cultivable have been dissected by deep cracks and collapsed tunnels, making mechanization and even manual cultivation impossible, and the terrains often become inhospitable for human settlement (Chibuogwu and Ugwu, 2023b). The development of these subsurface tunnels has also fundamentally altered the hydrogeological cycle of the affected areas. The natural groundwater flow paths are short-circuited, and perched aquifers are drained through the pipe networks. Consequently, open wells and shallow boreholes that previously yielded water throughout the year have become unsustainable and dry up even during peak rainy seasons, thereby exacerbating water scarcity (Ekenkwen, 2010; Nich and Okeke-Ogbu, 2017).

In many of these events, there have been socio-economic consequences, including loss of lives and properties, destruction of road networks, and disruption of people's daily livelihoods. Farmlands, residential buildings and critical infrastructure have been swallowed by sudden ground collapse, cutting short the embedded socio-economic activities of the affected populations (Nich and Okeke-Ogbu, 2017). In an attempt to reclaim roads, salvage properties and restore valuable farmlands, huge financial resources have been sunk by both affected communities and the state government (Uchegbu, 2004; Nich and Okeke-Ogbu, 2017).

While previous studies have largely focused on surface mapping and descriptive accounts of soil piping and subsidence, limited attempts have been made to characterize the subsurface geometry and depth of these pipes using geophysics. The patching method currently in use has failed precisely because the subsurface extent remains unknown. It is against this backdrop that the present study attempts to use an integrated geophysical approach, involving Vertical Electrical Sounding (VES) and Magnetic surveys, to investigate soil pipes in a sinkhole site at Awka South Local Government Area of Anambra State, Nigeria. This integrated approach is expected to provide non-invasive, high-resolution imaging of the subsurface pipes, delineate zones of low compaction and collapsed materials, and provide scientific baseline data for effective remediation design, rather than the trial-and-error patching method.

1.1 Study Area

The study was carried out in two sinkhole-affected sites in Awka South Local Government Area of Anambra State, Nigeria (Figure 1). Awka South LGA lies between Latitudes 6°05'N to 6°20'N and Longitudes 7°00'E to 7°12'E within the tropical rainforest zone. The area is characterized by a tropical climate with distinct wet and dry seasons, with annual rainfall ranging from 1800 mm to over 2000 mm, most of which occurs between April and October.

Geologically, the location is situated in the Anambra Basin, which forms part of the Lower Benue Trough tectonic unit. Various researchers, such as (Reyment, 1958; Wright, 1968) have conducted detailed analyses of the regional stratigraphy and geology of the trough. The origin of the Anambra Basin can be traced back to the Santonian-Campanian tectonic episode, when there was a widespread tensional regime during the Cretaceous. This event led to the folding of the Abakaliki Anticlinorium and the formation of the Anambra Basin as a sedimentary depocentre (Reyment, 1958). The basin's sediments were deposited during the Cretaceous to Paleogene periods with a dominant NW-SE trend, and the beds gently dip towards the northwest.

Awka town and its surrounding areas are primarily underlain by the Imo Shale Formation. This shale is fine-textured and varies in colour from dark grey to bluish-grey, with some parts containing thin bands of clay-ironstone and sandstone, as shown in Figure 1. Towards the top, the Imo Shale becomes increasingly sandy and may contain alternating bands of sandstone and shale. The soils are predominantly weak, lateritic, acidic and poorly consolidated at depth, with sandy members that host prolific groundwater reservoirs (aquifers). When saturated, pore water pressures in these aquifers become high, making the overburden highly unstable.

Gully erosion, landslides and flooding have remained the most common and most studied environmental hazards facing Anambra State, particularly during the rainy season (Chibuogwu and Ugwu, 2023c). The state, which is largely underlain by the unconsolidated and highly erodible sands of the Nanka and Ameki Formations in its eastern and central parts, and the Imo Shale in Awka and environs, is naturally predisposed to severe denudation. The combination of dispersive soils, high rainfall intensity, poor drainage, and anthropogenic activities has exacerbated this vulnerability. In recent decades, a more concealed hazard, soil piping and land subsidence due to collapse of subsurface tunnel roofs, has become prominent in Awka South and neighbouring LGAs (Nich and Okeke-Ogbu, 2017). The lateritic and sandy soils are easily eroded by storm-water runoff, while subsurface seepage gradually washes away fine particles to form continuous pipes, leading to sudden sinkhole formation (Figure 2).

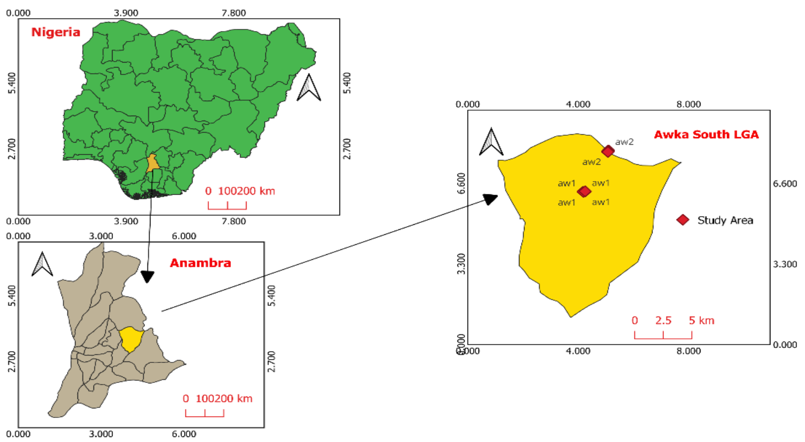

Figure 1: Map of the Study Area showing Vertical Electrical Sounding Location

Figure 2: Erosion in Awka (a) Soil pipe (b) Gully

2.0 Materials and methods

2.1 Direct Current (DC) Resistivity Method

The Direct Current (DC) resistivity method is a geophysical technique that involves the creation of an artificial electric field by injecting a direct current (I) into the subsurface through a pair of metallic electrodes known as the current electrodes or transmitter circuit (Carrazza et al., 2016). As a result of this injected current, an electrical potential field (ΔV) is established in the ground, which is then intercepted and measured by another pair of electrodes known as the potential electrodes or receiver circuit, which may be metallic or non-polarizable. Through the measurement of current and potential difference, the electrical properties of subsurface materials and the underlying geological conditions can be accurately investigated (Loke and Barker, 1996).

Data acquisition is achieved by repeated injection of current and measurement of the resulting potential, allowing for the determination of apparent resistivity of the subsurface. Lateral variations in resistivity provide information on heterogeneities related to mineralogical composition or geological structures such as faults, dykes, contacts, voids and saturated zones (Carrazza et al., 2016).

2.2 Vertical Electrical Sounding (VES) Method

For this study, Vertical Electrical Sounding (VES) was carried out using the Schlumberger electrode configuration (Olafisoye et al., 2013). The PASI resistivity meter was used to measure the apparent resistivity values. A total of eighteen (18) VES points were occupied (Figures 3 and 4) with a maximum half-current electrode spacing (AB/2) of 100 m, which is sufficient to investigate the shallow subsurface where soil pipes are prevalent.

The field data were first interpreted using the partial curve matching technique (Olafisoye et al., 2013), involving the use of master curves (Olafisoye et al., 2013) and auxiliary charts (Wilson et al., 2018) to obtain initial estimates of the resistivity and thickness of the geoelectric layers at each VES location. These initial geoelectric parameters were subsequently used as input models for computer-aided iterative inversion using the IPI2Win software. The partial curve matching and inversion revealed a 3 to 5-layer geoelectric model of alternating resistive-conductive-resistive layers for the eighteen VES locations, which is characteristic of interbedded laterite, clayey sand, saturated zones and void spaces associated with soil piping.

2.3 Isoresivity Map

Isoresistivity maps are plan-view maps that show the lateral variation of apparent resistivity or true resistivity at a constant electrode spacing (AB/2) or at a constant depth across the study area. They are essential for delineating lateral discontinuities such as soil pipes, voids, clay pockets and saturated zones. The isoresistivity maps for this study were generated using the following procedure:

From the eighteen (18) VES curves obtained, apparent resistivity values (ρa) at selected half-current electrode spacings were extracted. Commonly used AB/2 values for shallow piping investigation are 5 m, 10 m, 15 m, 20 m, 30 m, 45 m, 65 m and 100 m. These AB/2 values correspond approximately to increasing depth of investigation. In addition, inverted true resistivity values for specific depth slices, e.g., 2 m, 5 m, 10 m and 15 m depth, obtained from IPI2Win inversion, were also compiled for depth-slice isoresistivity maps.

The extracted resistivity values were tabulated against their geographic coordinates (Easting, Northing) for all VES points. The data were organized in Excel in the format: VES No., X (m), Y (m), ρa at AB/2 = 10 m, ρa at AB/2 = 20 m, ρa at AB/2 = 45 m, etc. The compiled data were imported into a contouring software, Surfer 13. The data were gridded using the Kriging or Minimum Curvature interpolation algorithm. Kriging is preferred because it provides unbiased estimation and accounts for spatial correlation of resistivity data.

2.4 Magnetic Method

For the total magnetic intensity (TMI) Ground magnetic data were acquired using a portable proton precession magnetometer with a sensitivity of 0.1 nT, alongside a GPS for navigation and positioning. A total of nine (9) profiles were established over the sinkhole site at approximately 2 m inter-profile spacing (Figure 2). Each profile

comprised 20 stations at a minimum spacing of 1 m, oriented in the North-South direction to form a 2 m x 2 m regular grid, ensuring high-resolution coverage of the piping zone.
To correct for temporal variations of the Earth's magnetic field, a suitable base station was established at a magnetically quiet location, far from cultural noise, buildings and any magnetic materials within the study area. Magnetic readings were recorded at the base station at 30-minute intervals throughout the survey period for diurnal correction. The diurnal correction was achieved by subtracting the temporal variation recorded at the base station from the corresponding field measurements taken at the grid stations.
The diurnally corrected data were gridded using the minimum curvature interpolation algorithm to produce a smooth and continuous magnetic field surface, and plotted using the Origin software package. Due to the limited areal extent of the study area, typically less than 100 m x 100 m, corrections for the International Geomagnetic Reference Field (IGRF) and regional-residual separation were not considered, as their effects are negligible at such small survey scales.

3.0 Result

3.1 Vertical Electrical Sounding

Table 1: VES Results for Awka Site I

VES	Northing	Easting	ρ(Ω.m)	∑ρ <5m (Ω.m)	Depth	Thickness	Curves
1	691349	786263	5229	78549	1.28	1.28	
			1414		2.72	1.43	HKQ
			71906		4.62	2.9	
			6510		83.5	77.9	
			531				
2	691379	786373	60.8	16122.7	0.5	0.5	HKH
			12.2		0.92	0.42	
			16015		1.23	0.314	
			34.7		3.28	2.04	
			18.21				
3	691411	786494	2517	23132	0.5	0.5	KHK
			19064		0.911	0.411	
			1551		2.11	1.26	
			25146		7.76	5.6	
			262				
4	691366	786242	130	24460.9	0.5	0.5	HK
			22.9		0.387	0.887	
			24308		0.578	1.47	
			2528				
5	691403	786364	16248	97221	0.5	0.5	KHK
			80973		1.39	0.885	
			27151		10.71	9.29	
			5117		82.1	71.5	
			1284				
6	691440	786479	2515	11254	0.839	0.839	AKQ
			8739		4.32	3.48	
			37448		8.85	4.53	
			7462		84	75.2	
			179				
7	691397	786242	3.04	16.369	2.02	2.02	KHA
			12.7		1.86	3.88	
			0.629		3.45	7.33	
			1.75		69.2	76.6	
			164				
8	691429	786363	56.2	66.8	1.59	1.59	HKH
			10.6		3.52	1.94	
			212		11.6	8.04	
			18.3		38.2	26.4	
			4407				
9	691458	786406	24.5	30.59	1.05	1.05	HA
			6.09		3.09	2.04	
			650		69.3	66.3	
			1605				

The resistivity dataset table 1 and figure 3 provides information into understanding soil erosion processes, subsurface piping susceptibility, and slope stability across the study area. Electrical resistivity is closely linked to soil texture, cohesion, and moisture retention, making it a reliable indicator for distinguishing between highly erodible sandy formations and impermeable clay or shale boundaries.

At VES 1, 3, 5, and 6, the topsoil and shallow subsurface layers exhibit exceptionally high resistivity values ranging from 2,515 to 16,248 Ω·m. These high resistivity horizons correspond to porous, dry, non-cohesive Nanka Sands. With minimal clay binding and high inter-granular porosity, these sands lose shear strength when saturated, leaving them highly vulnerable to hydraulic detachment, that could result to soil piping, gully wall collapse, and rapid erosion under concentrated runoff. The shallow intermediate layers at VES 2, 4, 7, 8, and 9 record much lower resistivities, between 6.09 and 22.9 Ω·m, with VES 7 reaching a minimum of 0.629 Ω·m at 3.45 m depth. These conductive horizons represent saturated clay or shale lenses with high water-dispersible clay content.

The sounding curves HK and HKH configurations at VES 1, 2, 4, and 8 reveal a high–low–high resistivity sequence, indicating a moisture-retentive intermediate horizon sandwiched between more resistive layers. This arrangement promotes lateral subsurface flow, and soil piping, which are key drivers of headward gully retreat in southeastern Nigeria. KHK profiles at VES 3 and 5 show alternating resistive sands and conductive interbeds, concentrating seepage forces along headwalls and causing severe undercutting and slope collapse. Meanwhile, KHA and HA curves at VES 7 and 9 reflect shallow, clay-dominated profiles that lose structural integrity under wet conditions, leading to sheet erosion and rill development.

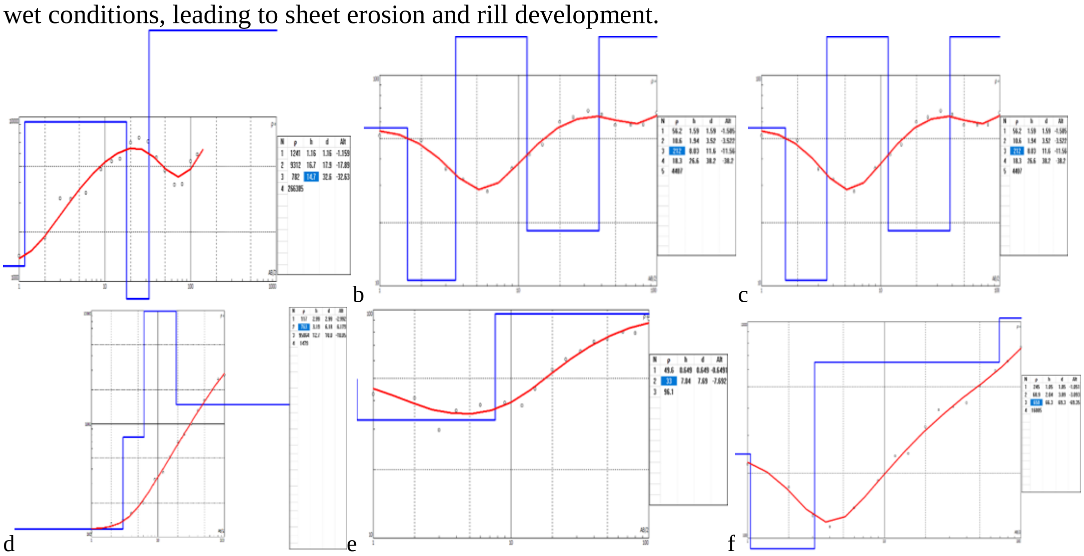

Figure 3: Sample of VES results at both Awka site 1 (a-c) and Awka site II (d-f)

The geoelectrical profile across VES 10 to VES 18 reveals lateral and vertical variability (Figure 3 and Table 2). VES 10, 16, 17, and 18 exhibit elevated topsoil and shallow subsoil resistivities, ranging between 1078 and 4020 Ω·m, with subsurface sand units at VES 17 and 18 reaching 14,219 Ω·m and 9312 Ω·m respectively. These highly resistive, coarse-grained, friable sands are characterized by negligible cohesion and low shear strength when saturated. Where such formations form possible cavity, rainfall impact energy drives rapid particle detachment, severe gully expansion, and cantilever-type mass failure.

In contrast, VES 12, 13, 14, and 15 record much lower shallow resistivities, generally less than or equal to 347 Ω·m. VES 14 drops sharply to 9.47 Ω·m at a depth of 1.37 m, while VES 13 shows a second-layer resistivity of 33.0 Ω·m. These conductive horizons correspond to clay- and silt-rich lenses that act as aquitards. During intense storm events, infiltrating water accumulates at these clay interfaces, producing sharp contrasts in hydraulic conductivity.

Curve configurations further illustrate active subsurface erosion mechanisms. VES 14 and VES 16 display HK curve signatures, marked by a high–low–high resistivity sequence in which a conductive, moisture-retentive intermediate horizon is sandwiched between resistive layers. This arrangement accelerates subsurface piping by channeling lateral seepage flow through the incompetent horizon, undermining upper soil layers and triggering sudden subsidence. Similarly, HA and KA curve types at VES 17 and 18 reveal deep, interlayered resistive sands overlying moderately conductive horizons before encountering indurated basement or sandstone beds with resistivities exceeding 31,000 Ω·m. This stratification concentrates hydraulic gradients along internal contacts, creating persistent conduits for tunnel erosion.

Table 2: VES Results for Awka Site II

VES	**Northing**	**Easting**	**ρ(Ω.m)**	**∑ρ at <5m (Ω.m)**	**Depth**	**Thickness**	**Curves**
10	695171	787995	1078	3432	0.5	0.5	AK
			2354		3.58	3.08	
			54228		5.65	2.07	
			1891				

11	695413	788039	117	117	2.99	2.99	AK
			763		6.18	3.19	
			95054		18.8	12.7	
			1479				
12	695683	788123	47.5	29898.5	1.58	1.58	AK
			146		1.83	3.41	
			29705		2.76	6.61	
			70.5				
13	695177	788154	49.6	49.6	0.649	0.649	H
			33		7.69	7.14	
			96.1				
14	695376	788187	347	356.47	1.37	1.37	HK
			9.47		1.68	0.306	
			31594		6.75	5.07	
			96.8				
15	695707	788241	250	316.8	0.709	0.709	K
			66.8		2.24	2.24	
			45.36				
16	695231	788325	4020	5014	0.665	0.665	HK
			994		1.61	0.943	
			59961		9.18	7.5	
			1931				
17	695467	788363	2355	2355	0.692	0.692	HA
			14219		17.5	16.8	
			1522		34.8	17.3	
			31814				
18	695774	788400	1241	1241	1.16	1.16	KA
			9312		16.7	17.9	
			782		14.7	32.6	
			266305				

3.2 Isoresistivity Mapping

To delineate the spatial geometry, lateral continuity, and preferred migration pathways of active soil piping networks, true isoresistivity maps were constructed for the critical subsurface interval (Figures 4). The vertical electrical soundings (VES), confirms that hydraulic piping in the study area is a shallow-seated phenomenon, initiating predominantly within the uppermost vadose zone (Gibson et al., 2004; Mi et al., 2013; Li et al., 2015; Got et al., 2020; Joshi et al., 2021; Borah et al., 2022). Hence, for this study the resistivity map was analysed from a depth of approximately 5m

The resistivity distribution for Awka Site I (Figure 4a) exhibits a wide dynamic range, spanning from baseline conductive values below, represented by deep blue contours, to extreme resistive peaks exceeding depicted as magenta and pink closures. The map is dominated by a pronounced, anticlinal-like high-resistivity contour closure centered around VES 5, which extends southwestward toward VES 1. This continuous, elongated high-resistivity delineates a partially desaturated subsurface pipe system where the ultra-high resistivity signature reflects subsurface air voids and loose, highly porous sand infill within the conduit core. Furthermore, the sharp lateral resistivity gradient toward the eastern margin at VES 7, 8, and 9 marks an abrupt transition into cohesive, moisture-retentive clayey-silt matrix, effectively restricting further lateral pipe expansion toward the east.

In contrast to the continuous linear ridge observed at Site I, Awka Site II (Figure 4b) demonstrates a distinct, localized structural geometry. The resistivity pattern features a tightly bounded, concentric domal high-resistivity anomaly localized around VES 3. This isolated closure delineates a major vertical-to-subhorizontal soil pipe inlet/outlet node where steep resistivity gradients radiate outward toward VES 6 in the northeast and VES 2 and 5 to the west, outlining the directional dispersal of preferential subsurface flow. Meanwhile, the surrounding western and northern areas at VES 1, 4, 7, and 8 maintain uniformly low resistivities below, indicating that internal piping at Site II may be structurally confined along the eastern sector by low-permeability fine-grained facies.

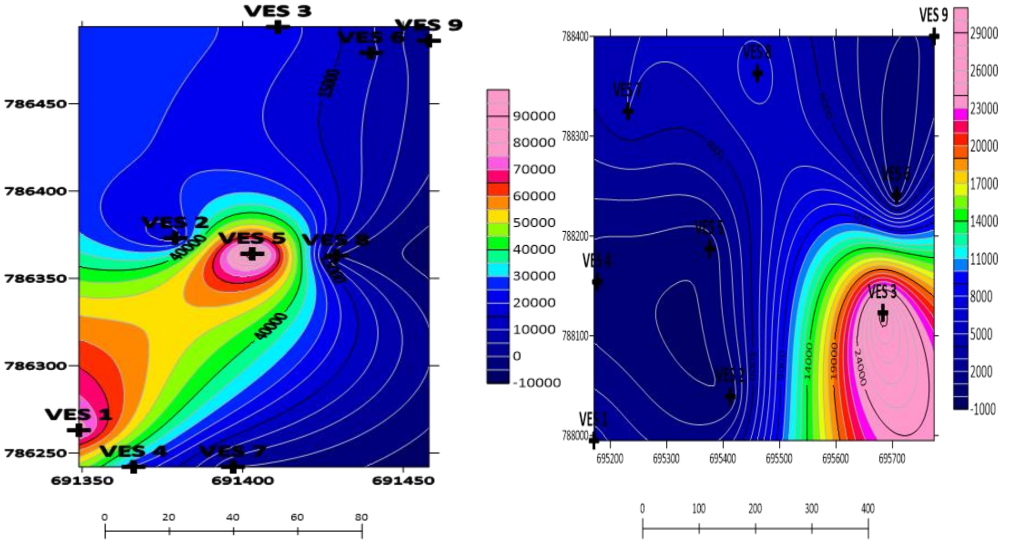

Figure 4: Isoresistivity Maps (a) Awka Site I (b) Awka Site II

3.3 Topographic and Geomagnetic Anomaly Distribution at Awka sit 1

The high-resolution digital elevation contour map for Awka Site I (Figure 5) delineates a highly dynamic topographic surface with elevations ranging from 47 m to over 72 m above mean sea level across coordinates 6.2348° N to 6.2358° N and 7.0822° E to 7.0827° E. Topographic contours are densely packed along a prominent, central linear corridor trending SW–NE. This steep elevation gradient is defined by a narrow, high-elevation ridge reaching 67–72 m that immediately borders a sharp drop into lower terrain at 47 m along the northwestern and southeastern flanks.

The extreme contour density along this SW–NE trend marks an active morpho-structural gully wall and headcut zone. Slope steepness in this central sector generates substantial hydraulic energy during heavy precipitation events. Surface runoff is funneled down these steep gradients, concentrating hydraulic head along the valley axis. This topographic configuration directly drives gravity-induced infiltration into friable topsoil, providing the mechanism necessary to initiate subsurface piping along the same SW–NE corridor identified in the geoelectrical surveys.

The total magnetic intensity (TMI) anomaly map for Awka Site I displays pronounced field variations, spanning values from −196.0 nT (deep blue depressions) to +91.00 nT (intense red and grey closures). The spatial configuration of these magnetic responses reflects significant lateral variations in subsurface lithology, iron mineralization, and degree of weathering.

Strong positive magnetic anomalies (+55.13 to +91.00 nT), appearing as localized closures in the central and northern sectors, represent shallow, iron-rich lithologies typical of the Nanka Formation, including ferruginous sandstones, ironstone indurated caps, or heavy-mineral sand lenses. Conversely, prominent magnetic lows (−124.3 to −196.0 nT) correspond to heavily leached, weathered sand matrices, water-saturated zones, or subterranean piping voids where magnetic mineral susceptibility has been reduced or removed by internal erosion.

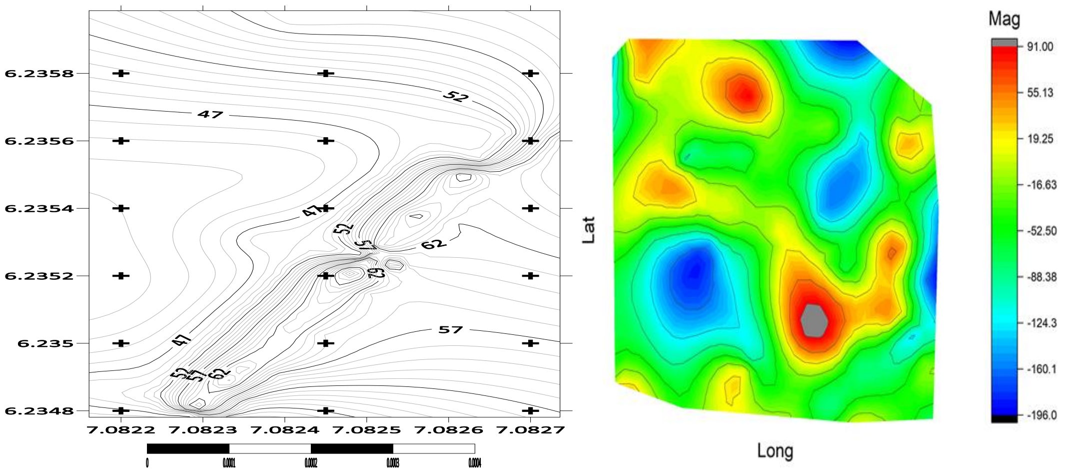

Figure 5: Topographic and Geomagnetic Anomaly Distribution at Awka sit I

Topographic and Geomagnetic Anomaly Distribution at Awka sit II

The topographic elevation contour map for Awka Site II delineates an elongated, highly structured surface topography spanning coordinates 6.2348° N to 6.2358° N and 7.0822° E to 7.0827° E (Figure 6). Surface elevations rise significantly across this site, with contour levels exceeding 125 m and reaching prominent linear crests above 150 m. The defining feature of this map is a narrow, continuous, and tightly packed contour band trending along a SW–NE linear axis. The high contour density along the margins of this feature indicates extremely steep sidewall gradients flanking a central valley or headcut trough like is seen in Awka site 1. This steep topographic relief generates high potential energy during rain events, funneling surface runoff directly into the central SW–NE channel. This concentrated overland flow creates intense shear stresses along the slope face, driving rapid surface wash and supplying the hydraulic head necessary to recharge shallow subsurface flow paths. The TMI anomaly map for Awka Site II exhibits a broad dynamic range, with field values spanning from −374.0 nT (represented by deep blue and black depressions) to +164.0 nT (depicted as intense red and grey closures). This wide variation highlights significant sub-surface lithological contrasts, structural fracturing, and variable iron mineralization within the underlying Nanka Formation. Prominent magnetic highs ranging from +29.50 nT to +164.0 nT appear as discrete closures in the south-central (marked by a distinct grey core) and north-northeastern sectors. These high-intensity responses represent near-surface, indurated ironstone capping layers and highly oxidized, ferruginous sandstone beds. Conversely, deep magnetic lows from −172.3 nT down to −374.0 nT dominate the southwestern and central-western quadrants. These negative anomalies delineate zones of severe chemical leaching, high subsurface moisture saturation, or subterranean air-filled piping voids where magnetic mineral susceptibility has been depleted.

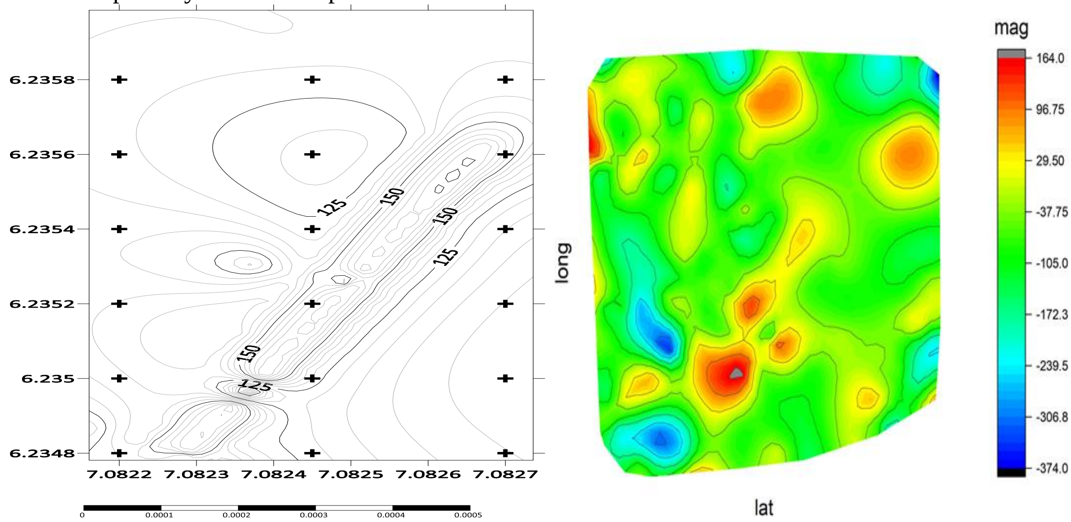

Figure 6: Topographic and Geomagnetic Anomaly Distribution at Awka sit II

4.0 Discussion

VES and Geoelectric Characteristics

Eighteen VES points reveal a 3–5 layer resistive–conductive–resistive succession typical of laterite, clayey sand or saturated zones, and weathered sand. The curve types HK, HKH, KHK, AK, AKQ, and HA are characteristic of Imo Shale and Nanka Sand interbedding.

The diagnostic parameter Σρ at <5 m is critical in differentiating subsurface conditions (mi et al., 2013). Active pipe zones such as VES 7, 8, 9, 13, and 15 show extremely low Σρ values of 16.36, 66.8, 30.59, 49.6, and 316.8 Ω.m. For instance, VES 7 records 3.04 Ω.m at 2.02 m depth with a KHA curve, indicating water-saturated, clay-filled pipes and leached zones. Collapsed or dry void zones, including VES 1, 3, 5, 10, 16, 17, and 18, display anomalously high Σρ values. VES 1 registers 78,549 Ω.m and VES 5 reaches 97,221 Ω.m, with topsoil resistivities of 5229 Ωm and 16,248 Ωm respectively. These values are typical of air-filled voids and dry collapsed sand formations. Also Chibuogwu and Ugwu, (2023b), and Chibuogwu and Ugwu (2023d)) have correlated the study area with bore hole log to show the soil profiles of the study area.

Transitional zones such as VES 2, 4, 6, 11, 12, and 14 exhibit moderate Σρ values ranging from 16,122 to 29,898 Ω.m with alternating layers. VES 6, for example, shows an AKQ curve with 2515 Ω.m in the topsoil, 37,448 Ω.m at 8.85 m depth, overlying a 179 Ω.m horizon, representing an intact cap above a water-filled pipe. Piping is predominantly shallow, occurring between 0.5–3.5 m depth, with roof thicknesses as low as 0.649 m in VES 13. This explains the sudden catastrophic subsidence observed in the study area (Ezenkwen, 2010; Ajayi and Okafor, 2025) gave similar result in their study.

Topography and Surface Expression of Piping

The topographic maps of Awka Site I and II demonstrate that soil piping and sinkhole development in Awka South is strongly topographically controlled. Site I is characterized by a highly dissected micro-relief with elevations of 38 m to 58 m over a short distance. Tightly packed contours forming a closed central depression represent the surface expression of a collapsed pipe roof. The steep gradients on the flanks generate high runoff velocity and shear stress during rainfall, which erodes the weak, poorly consolidated lateritic topsoil. This runoff is funnelled into tension cracks and pipe inlets, providing the hydraulic head that drives subsurface erosion.

Site II exhibits a more evolved stage, displaying an elongated SW-NE trending trough with elevations above 150 m and very steep sidewalls. This morphology indicates coalescence of isolated sinkholes into a continuous gully-like pipe channel. The persistent SW-NE orientation corresponds to the regional structural trend of the Anambra Basin and groundwater flow direction, suggesting that piping exploits preferential structural weaknesses and slope.
Magnetic Anomaly and Subsurface Lithology
Ground magnetic data reveal the degree of weathering, iron depletion and void development.
In Site I, (TMI) ranges from -196.0 nT to +91.0 nT. Localized positive anomalies of +55.13 to +91.00 nT in the central and northern sectors correspond to shallow, iron-rich indurated layers of the Nanka Formation, including ferruginous sandstones and ironstone caps that form resistant pipe roofs. Pronounced magnetic lows of -124.3 to -196.0 nT correlate spatially with the topographic depression and indicate zones where magnetic minerals have been leached by prolonged seepage, or where water-saturated and air-filled voids exist. These are interpreted as active piping zones.
Site II shows a wider range of -374.0 nT to +164.0 nT, reflecting greater heterogeneity and more mature piping. High closures of +29.5 to +164.0 nT in the south-central and north-northeastern parts represent preserved ironstone lenses. Extremely deep lows of -172.3 to -374.0 nT in the southwestern and central-western quadrants cannot be explained by lithology alone; they delineate extensive subsurface voids, saturated pipes and severely leached sands where susceptibility is completely depleted. The limited survey extent (<100 m x 100 m) justifies the non-application of IGRF and regional-residual corrections, as the target is local contrast.
Therefore, this integrated geophysical investigation demonstrates that Vertical Electrical Sounding (VES), topographic analysis, and ground magnetic surveys may be utilized to provide complementary information into piping processes and lithological variations in Awka South. The VES results reveal distinct geoelectric signatures that differentiate active, transitional, and collapsed pipe zones, with shallow depths (0.5–3.5 m) explaining the sudden subsidence events observed. Topographic mapping confirms that piping and sinkhole development are strongly controlled by terrain morphology, slope gradients, and regional structural trends of the Anambra Basin.
Magnetic anomaly analysis further highlights the role of iron-rich indurated layers in forming resistant pipe roofs, while pronounced magnetic lows delineate zones of leaching, saturation, and void development. Together, these findings establish that piping in the study area is both structurally and lithologically controlled, with shallow roof thicknesses making the terrain highly susceptible to catastrophic collapse.

5.0. Conclusion

This study has successfully investigated subsurface soil pipes in sinkhole-affected sites in Awka South LGA of Anambra State using integrated Vertical Electrical Sounding (VES) and ground magnetic methods.
Topography analysis shows steep, dissected slopes with central depressions and SW-NE trending troughs that concentrate runoff into pipe inlets, sustaining erosion. Magnetic data delineated two zones: highs of +29.5 to +164.0 nT representing intact ferruginous sandstone/ironstone pipe roofs, and lows of -124.3 to -374.0 nT indicating leached zones, water-saturated pipes and air-filled voids. Site II shows more extensive piping.
VES revealed 3-5 layer resistive-conductive-resistive models with HK, HKH, KHK and AK curves. Very low Σρ <5m of 16.36-66.8 Ωm (VES 7,8,9,13) indicates active water-saturated pipes, while very high Σρ of 78,549-97,221 Ωm (VES 1,5) indicates dry voids. Piping is shallow at 0.5-3.5m depth, with VES 13 showing roof thickness of 0.649m, indicating imminent collapse.
The integration of VES and magnetic data proves that soil pipes in Awka South are not isolated features but form an interconnected network trending SW-NE, controlled by lithological heterogeneity, structural weakness, and groundwater flow within the Imo Shale/Nanka Formation contact. This study has confirmed that the current patching method is ineffective because it does not address the lateral continuity and depth of the pipe network.

6.0 Recommendation

The Anambra State Government and community should discontinue the use of laterite backfilling and use lime solution to threat soil where soil are dispersed, since this occurs mainly at top soil with low conductivity government should reduce conductivity by filling area with high resistivity concentrated soils as a remediation technique. Geophysical evidence shows that pipes extend beyond the collapsed zone and patching only diverts water to create new pipes adjacent to the filled area. All active pipes delineated by magnetic lows and low resistivity zones should be excavated, compacted with non-dispersive clay, and treated with lime or cement stabilization to reduce soil dispersity.
Construction of subsurface cut-off drains and graded filters to intercept seepage flow and reduce pore water pressure that drives piping.

Acknowledgement

The authors deeply acknowledge the assistance of the staff of Anambra state material testing lab.

References

Ajayi, F. F., & Okafor, E. (2025). Geochemical and geotechnical characterization of colluvium soils of Nanka Area, as indicators and control of gully erosion within Anambra Basin, Nigeria. Discover Geoscience, 3(1), 178.

Borah, U. K., Gond, A., Rajan, P. P., Sivan, R., & Vivekanandan, N. (2022). Joint geomorphological and geophysical (electrical resistivity) investigation for the configuration of soil pipe. Contributions to Geophysics and Geodesy, 52(2). https://doi.org/10.31577/congeo.2022.52.2.4

Carrazza, L., Moreira, C., & Portes, L. (2016). Gully cavity identification through electrical resistivity tomography. Revista Brasileira de Geofísica, 34. https://doi.org/10.22564/rbgf.v34i2.799

Chibuogwu, I. U., & Ugwu, G. Z. (2023). Investigating the Susceptibility of Tunnel Erosion in Southern Nigeria using Integrated Geophysical Methods.

Chibuogwu, I. U., & Ugwu, G. Z. (2023a). An Open Investigation of Some Soil Pipes Forming Soil Subsidence at Awka South Local Government Area Using Very Low Frequency Electromagnetic Geophysical Technique. International Journal of Scientific Research in Multidisciplinary Studies, 9(2), 40–45.

Chibuogwu, I. U., & Ugwu, G. Z. (2023b). Examining Tunnel Erosion Using Vertical Electrical Sounding and Ground Magnetic Geophysical Techniques in Awka, Nigeria. International Journal of Geography, Geology and Environment, 5, 111-121.

Chibuogwu, I. U., Ugwu, G. Z., & Egwuonwu, G. N. (2023). Conducting a Comprehensive Physical Investigation on Uncontrolled Internal Soil Erosion Leading to Sinkholes in Anambra State, Nigeria. Asian Journal of Geographical Research, 6(3), 104-122.

Ezenkwen, E. (2010). Gully Erosion in Anambra State: Nnaka. Patrotic Union Journal, 1, 9–18.

Gibson, P. J., Lyle, P., & George, D. M. (2004). Application of Resistivity and Magnetometry 1 Geophysical Techniques for Near-Surface Investigations in Karstic Terrains in Ireland. Journal of Cave 2 and Karst Studies, 66, 35–38.

Got, J. -B., Bielders, C. L., & Lambot, S. (2020). Characterizing soil piping networks in loess-derived soils using ground-penetrating radar. Vadose Zone Journal, 19(1). https://doi.org/10.1002/vzj2.20006

Joshi, M., Prasobh, P. R., Rajappan, S., Rao, B. P., Gond, A., Misra, A., Eldhose, K., Nandakumar, V., & Tomson, J. K. (2021). Detection of soil pipes through remote sensing and electrical resistivity method: Insight from southern Western Ghats, India. Quaternary International, 575–576, 51–61. https://doi.org/10.1016/j.quaint.2020.08.021

Li, S., Liu, B., Nie, L., Liu, Z., Tian, M., Wang, S., Su, M., & Guo, Q. (2015). Detecting and monitoring of water inrush in tunnels and coal mines using direct current resistivity method: A review. Journal of Rock Mechanics and Geotechnical Engineering, 7(4), 469–478. https://doi.org/10.1016/j.jrmge.2015.06.004

Loke, M. H., & Barker, R. D. (1996). Rapid least-squares inversion of apparent resistivity pseudosections by a quasi-Newton method1. Geophysical Prospecting, 44(1), 131–152. https://doi.org/10.1111/j.1365-2478.1996.tb00142.x

Mi, K. P., Samgyu, P., Myeong-Jong, Y., Changryol, K., Jung-Sul, S., Jung-Ho, K., & Adepelumi, A. A. (2013). Application of electrical resistivity tomography (ERT) technique to detect underground cavities in a karst area of South Korea. Environ Earth Sci, 50(2), 256–267.

Nich, O., & Okeke-Ogbu, C. J. (2017). Erosion Problems and their impact in Anambra State, Nigeria (A case study of Nnaka Community). International Journal of Environment and Pollution Research, 5, 24–87.

Olafisoye, E. R., Sunmonu, L. A., Adagunodo, T. A., & Oladejo, O. P. (2013). Groundwater contaminant's investigation at aarada waste disposal site using geophysical and hydro-physicochemical approach. IOSR Journal of Environmental Science, Toxicology and Food Technology, 2(4), 01-10.

Reyment, R. A. (1956). On the stratigraphy and palaeontology of the Cretaceous of Nigeria and the Cameroons, British West Africa. Geologiska Föreningen i Stockholm Förhandlingar, 78(1), 17-96.

Uchegbu, J. N. (2004). The role of Government and Citizens in Erosion Control, in H.C Mbah et al: Management of Environmental Problems and Hazard in Nigeria. Ashgate Publishing LTD Cower House. Croft Road Aldrshot Gill 3HR England.

Wilson, G. V., Wells, R., Kuhnle, R., Fox, G., & Nieber, J. (2018). Sediment detachment and transport processes associated with internal erosion of soil pipes: Sediment detachment and transport in soil pipes. Earth Surface Processes and Landforms, 43(1), 45–63. https://doi.org/10.1002/esp.4147

Wright, J. B. (1968). Deep crustal origin for oligoclase and andesine phenocrysts in basalt from Gombe, Nigeria. Nature, 218(5138), 262-263.